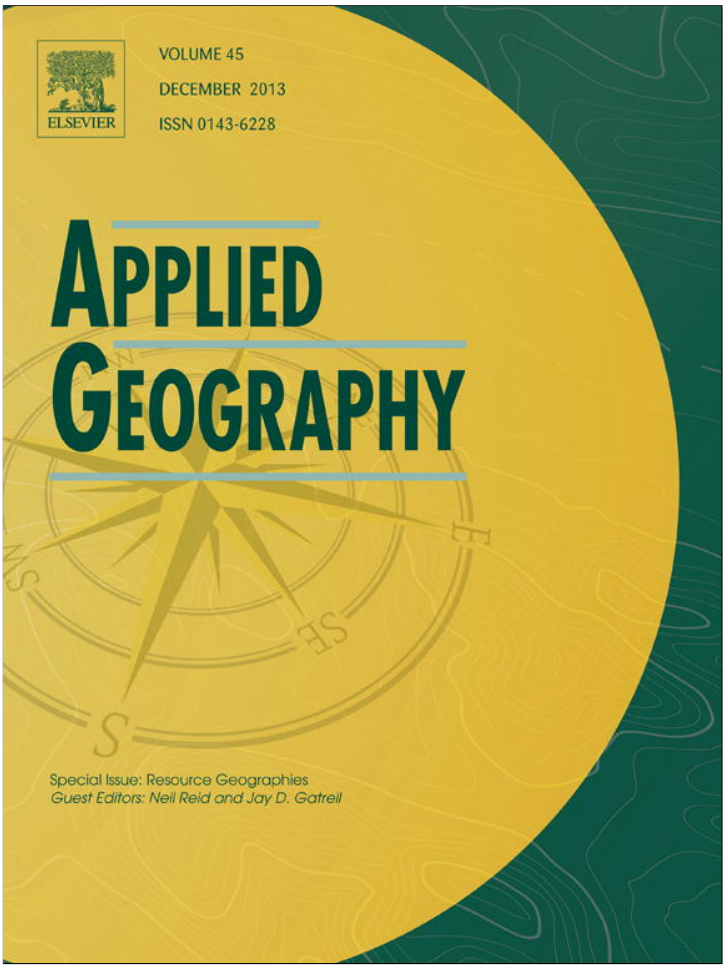

Applied Geography 45 (2013) 10–21

Contents lists available at ScienceDirect

Applied Geography

journal homepage: www.elsevier.com/locate/apgeog

Analyzing land-cover change and corresponding impacts on carbon budget in a fast developing sub-tropical region by integrating MODIS and Landsat TM/ETM+ images

Yimin Chen [a,b], Xia Li [a,b,*], Xiaoping Liu [a,b], Bin Ai [b,c]

[a] School of Geography and Planning, Sun Yat-sen University, Guangzhou, China
[b] Guangdong Key Laboratory for Urbanization and Geo-simulation, Sun Yat-sen University, Guangzhou, China
[c] School of Marine Sciences, Sun Yat-sen University, Guangzhou, China

Keywords:
Mixed-label analysis
Land-cover change
Carbon budget
MODIS
Landsat

A B S T R A C T

Land-cover change has significant impacts on regional carbon dynamics. Understanding the carbon consequences of land-cover change is necessary for decision makers to address the issues of carbon reduction and climate change mitigation. Optical remote sensing images have been widely used for detecting regional land-cover change. However, it is difficult to acquire desirable images for regions that are frequently affected by cloudy and rainy weather. In this study, we proposed an approach to deal with this problem by integrating moderate-resolution imaging spectroradiometer (MODIS) and Landsat images based on the mixed-label analysis (MLA) model. We tested this model in Guangdong Province, a fast developing sub-tropical region in China, to derive the provincial land-cover data for the analysis of land-cover change between 2000 and 2009 and its impacts on regional carbon dynamics. Results show that forest land decreased by 3.03%, while built-up area rapidly expanded by 73.01% from 2000 to 2009. The regional vegetation carbon sink declined by 2.6%, whereas the regional carbon emissions increased by more than 100% due to the fast urbanization and economic development. The regional vegetation carbon sink can only offset 4.1% of total carbon emissions in 2009, far below the national level (about 7.0–7.7%) at the same period. Future efforts to improve the regional carbon budget should focus more on the control of land development and the advance of energy efficiency.

Introduction

Human-driven land-cover change has profound impacts on the earth's ecosystems. A better understanding of the dynamics of land-cover change is fundamental for research on global environmental change and sustainability (Turner, Lambin, & Reenberg, 2007). Land-cover change can alter the regional patterns of carbon sink/source and further affect the global carbon cycle (Liu, Loveland, & Kurtz, 2004). The earth's terrestrial ecosystems play a key role in global carbon sink. It is estimated that terrestrial ecosystems have absorbed about 25% of the carbon emissions caused by human activities (Canadell et al., 2007). The world's urbanized areas, which are experiencing dramatic land-cover change, consume most of the global energy and become the major source of carbon emissions (Hutyra, Yoon, Hepinstall-Cymerman, & Alberti, 2011). The annual fluxes of carbon into (carbon sink) and out (carbon emissions) of a region is usually referred to as regional carbon budget (Potter, 2010). Assessing the impacts of land-cover change on regional carbon budget is of great importance for climate change mitigation and associated policy making, especially for those fast developing areas in the world.

Remote sensing has been widely used for analyzing regional land-cover change and its carbon consequences (Evrendilek et al., 2011; Hutyra et al., 2011; Latifovic, Zhu, Cihlar, Giri, & Olthof, 2004). Among the sources of optical images, the Landsat series (MSS, TM, and ETM+) are most frequently used because of their global coverage, long time span (more than 30 years), and user-community familiarity in terms of image processing and analysis (Redo & Millington, 2011). The relatively long revisit time (about 16 days) of the Landsat satellites, however, makes it difficult to acquire good-quality data in the areas of cloudy and rainy weather. This

* Corresponding author. School of Geography and Planning, Sun Yat-sen University, 135 West Xingang RD., Guangzhou 510275, PR China. Tel.: +86 13924203023; fax: +86 (020) 84115833.
E-mail addresses: gp04chym@mail2.sysu.edu.cn (Y. Chen), lixia@mail.sysu.edu.cn, lixia@graduate.hku.hk (X. Li).
URL: http://www.geosimulation.cn/

0143-6228/$ – see front matter © 2013 Elsevier Ltd. All rights reserved.
http://dx.doi.org/10.1016/j.apgeog.2013.08.002

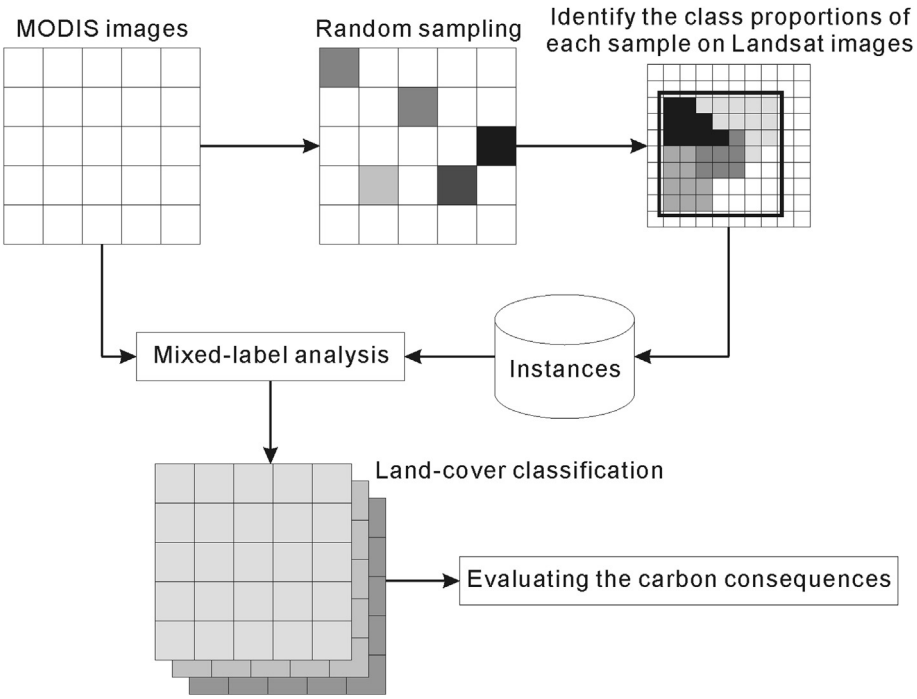

Fig. 1. Land-cover classification using the MLA model.

problem may become more severe if the application requires multiple scenes of images for the same date/season. Leckie (1990) found that in some humid regions of Canada, the chance of acquiring cloudless Landsat images even for a year is less than 10%. By contrast, images produced by the moderate-resolution imaging spectroradiometer (MODIS) have a wider single-scene coverage and shorter revisit time (1 day). Such advantages increase the possibility of acquiring cloud-free data for land-cover mapping in large areas (Friedl et al., 2002). The major drawback of MODIS images is their low spatial resolution, which to some extent limits the accuracy of land-cover classification (Wessels et al., 2004). It is expected that the integration of MODIS and Landsat images can provide a better land-cover classification for large and rainy areas.

The integration of MODIS and Landsat images for land-cover classification can be fulfilled in two ways. The first one is to generate a new image with MODIS's temporal resolution and Landsat's 30-m spatial resolution through image fusion models, such as the spatial and temporal adaptive reflectance fusion model (STARFM) proposed by Gao, Masek, Schwaller, and Hall (2006). This model is very useful for applications that require images with both high temporal and spatial resolution. However, the accuracy of this model might decrease if high spatial heterogeneity exists, or significant land-cover change occurs on the ground (Hilker et al., 2009). The second way of image integration is to collect high-quality training samples from Landsat images to feed the models for the classification of MODIS images. MODIS images have a wide areal coverage, which increases the difficulty of collecting high-quality training samples for classification. In fact, Landsat images can greatly facilitate the sample collection procedure. For instance, Sulla-Menashe et al. (2011) established the training sites for the classification of MODIS images through the manual interpretation of Landsat images. Redo and Millington (2011) also considered Landsat images as an important complementary data source for the classification of MODIS images.

If the second way is adopted, there are still problems on how to effectively embed the information from Landsat into the model to classify MODIS images as the spatial resolutions of these two image sources are far too different. Many models for the classification of MODIS images are developed based on the decision tree algorithm or its variations. These models are referred to as hard classification models, because they assume that all unclassified pixels are pure and only belong to (or are labeled as) one of the given classes/labels (Foody, 1997). Apparently this assumption is invalid for MODIS images as they usually have a lot of mixed-pixels due to the coarse spatial resolution. It is very likely that a pixel on MODIS images can contain more than just one land-cover type. Actually, the performance of hard classification models is rather limited when classifying MODIS images because of the contradiction between the assumption of pure-pixel and the existence of mixed-pixels on MODIS images. Moreover, as we will illustrate in our classification experiments (Section 4.1), hard classification models cannot effectively utilize the complementary information gained from Landsat images.

We alleviated such problem based on a recently developed mixed-label analysis (MLA) model (Liu, Li, & Zhang, 2010). This model belongs to the group of soft classification models, which allows for multiple and partial class membership properties of mixed-pixels (Foody, 2000). The MLA model employs a *k*-nearest neighbors (*k*-nn) algorithm to handle the complicated relationships between the land-cover composition and the observed spectra for mixed-pixels. Thus, the MLA model is more suitable to use than conventional hard classification models for MODIS images in terms of dealing with the mixed-pixel problem.

We selected Guangdong Province, a fast developing sub-tropical region in southern China, as the case study area. The large area of Guangdong is such that twelve scenes of Landsat images should be involved for covering the whole province. However, owing to the cloudy and rainy weather in Guangdong, it is very difficult to find all the overpassed Landsat images to be cloudless on similar acquisition dates. By contrast, only a single scene of MODIS image can cover the entire study area. The daily revisit time of MODIS images also increase the chance of acquiring cloudless data.

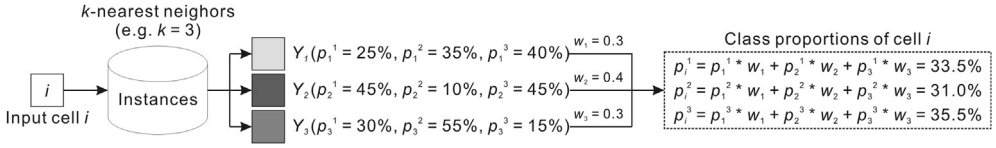

Fig. 2. Determining the land-cover proportions of an unclassified pixel using the MLA model ($k = 3$).

Therefore, we used the MLA model to integrate Landsat and MODIS images for the derivation of land-cover information.

Based on the derived provincial land-cover data, we also explored the impacts of land-cover change on the carbon budget of Guangdong. Recently Guangdong becomes the most populous province and the biggest economy among all provincial level divisions in China (W. Wang, Kuang, & Huang, 2011). Rapid land-cover change in Guangdong, particularly in the form of urban expansion, has been reported by many researchers (Li & Yeh, 2004; Seto et al., 2002; Shen, Wong, & Feng, 2002). The rapid urbanization causes the suppression of natural vegetation and the degradation of natural ecosystems (Lin et al., 2009; Liu, Li, Shi, & Wang, 2008; Sun et al., 2011). Additionally, the rapid urbanization also gives rise to the problems of increased energy consumption and carbon emissions (Chen, Li, Zheng, Guan, & Liu, 2011; Dhakal, 2009). Now Guangdong is the largest energy consumer and carbon emitter in China, and hence under a great pressure for achieving the goal of carbon reduction (Wang et al., 2011).

The procedures of our analysis on regional land-cover change and carbon budget are as follows: First, the land-cover data of Guangdong in 2000 and 2009 were produced by integrating MODIS and Landsat images through the MLA model. Second, the vegetation carbon sink was estimated based on the derived land-cover data; the carbon emissions were also calculated using the official statistical data. Finally, these results were used to evaluate the influences of land-cover change on regional carbon budget.

Methodology

Fig. 1 demonstrates the procedures of land-cover classification using the MLA model. First, pixel samples were randomly selected for the MODIS images (1500 samples for each year's MODIS image). Second, these samples were manually interpreted based on the available Landsat images to determine the land-cover types (including water, broad-leaved forest, coniferous forest, farmland, built-up area, bareland and shrubland) and their areal proportions within each pixel sample. Third, the pixel samples were divided into two groups: one was used to establish the instance library required by the MLA model, while the other was served as the test data. Finally, the MLA model was implemented for the classification of MODIS images. These results were used to analyze the impacts of land-cover change on regional carbon budget.

Mixed-label analysis (MLA) model

In the MLA model, a label corresponds to a specific land-cover type. The number of labels is finite, which can be denoted as C. A pixel i is represented as $x_i = (a_i^1, \ldots, a_i^n)$, where a_i^n is the nth feature of pixel i. The proportion of each label (land-cover type) in pixel i is expressed as $Y_i = (p_i^1, \ldots, p_j^c)$, where p_i^c is the areal proportion of the cth label, and $\sum p_i^c = 1$. Y_i can be determined through the following equation:

$$Y_i = f(x_i) + u_i, \quad i = 1, \ldots, m \tag{1}$$

where u_i is the random error term and m is the number of image pixels.

The function of $f(x_i)$ can be established using the k-nearest neighbors (k-nn) algorithm: First, the distances in feature space were calculated for the unclassified pixel i and all the known instances (those samples in the instance library). The k nearest neighbors can then be determined based on the calculated distances. Second, the weights for each neighbor were calculated by converting the distances using the transition function. Finally, the land-cover proportions of pixel i (i.e., Y_i) were solved through the weighted sum of the land-cover proportions of each selected neighbor.

Specifically, re-denote the k-nn-based $f(x_i)$ as $\widehat{f}_m(x)$. Given a set of instances $T = \{(x_1, Y_1), (x_2, Y_2), \ldots, (x_m, Y_m)\}$, $\widehat{f}_m(x)$can be expressed as the following function:

$$\widehat{f}_m(x) = \sum_{j=1}^{m} W_j(x_1, x_2, \ldots, x_m) Y_j \tag{2}$$

where $W_j(x_1, x_2, \ldots, x_m)$ is a weighted function that evaluates the contribution from instance (x_j, Y_j) for estimating $\widehat{f}_m(x)$.

The weighted function should also meet the following conditions:

$$W_j(x_1, x_2, \ldots, x_m) \geq 0 \quad \sum_{j=1}^{m} W_j(x_1, x_2, \ldots, x_m) = 1 \tag{3}$$

The weights of each instance were then calculated using the following equation:

$$d_i = d(x_i, x) \sqrt{\sum_{q=1}^{n} \left(a_i^q - a^q\right)^2} \tag{4}$$

where a_i^q and a^q are the qth feature of pixel i and the compared instance, while n is the number of feature.

After the calculation of the distances between pixel i and all instances, the k nearest neighbors can be determined in terms of shortest distances. Then the weighted function $W_j(x_1, x_2, \ldots, x_m)$ can be formulated as follows:

$$W_j(x_1, x_2, \ldots, x_m) = \frac{e^{-d_j}}{\sum_{j=1}^{k} e^{-d_j}} \tag{5}$$

where k is the number of nearest neighbors.

After the weights of each neighbor were specified, the land-cover proportions of the unclassified pixel i can be determined by summing all the weighted land-cover proportions of the k nearest neighbors. To make it clearer, we provide an example in Fig. 2. It assumes that there are a total of three land-cover types ($C = 3$) and three nearest neighbors ($k = 3$). If the weights of these three nearest neighbors are w_1, w_2, and w_3, respectively, then the areal proportion of the first land-cover type for an inquiring pixel i is $p_i^1 = p_1^1 \times w_1 + p_2^1 \times w_2 + p_3^1 \times w_3$. The second and the third land-cover types of this pixel can be calculated in the same manner.

The indicator of root-mean-square-error (RMSE) is used to evaluate the classification errors. The RMSE of the ith land-cover type can be calculated as follows:

Table 1
Calorific values and carbon emission factors of different fuel types.

Type	Calorific value (KJ/kg, KJ/m^3)	Carbon emission factor (t-C/TJ)	Type	Calorific value (KJ/kg, KJ/m^3)	Carbon emission factor (t-C/TJ)
Raw coal	20,934	26.8	Kerosene	43,124	19.6
Secondary coal	26,377	26.8	Diesel oil	42,705	20.2
Other washed coal	8374	26.8	Fuel oil	41,868	21.1
Briquette coal	20,934	26.8	Liquefied petroleum gas	50,241	17.2
Coke	2847	29.5	Refinery gas	46,055	18.2
Coke oven gas	17,375	13	Natural gas	38,979	15.5
Other gas	5234	13	Other petroleum product	41,868	25.8
Crude oil	41,868	20	Other coking product	2847	29.5
Gasoline	43,124	20			

$$\mathrm{RMSE}_i = \sqrt{(1/N)\sum_{j=1}^{N}(p_i - \hat{p}_i)^2} \quad (6)$$

where RMSE_i is the RMSE of land-cover type i, while N is the number of pixels; p_i and $\hat{p}_i$represent the derived and actual proportions of the ith land-cover type, respectively. The overall classification error is the mean of all RMSE_i:

$$\mathrm{RMSE}_{\mathrm{overall}} = \frac{1}{C}\sum_{i=1}^{C}\mathrm{RMSE}_i \quad (7)$$

Estimating the regional carbon budget

We used carbon emissions and vegetation carbon sink to represent the regional carbon budget. Generally, there are many sources of carbon emissions, such as fossil fuels combustion, cement production, and biological respiration, etc. Soil carbon is the largest carbon pool in the world, but it also can become a carbon source under some conditions, such as fire, drainage and grazing that can cause the release of soil organic matters. However, recent studies reveal that the soil carbon in Guangdong is not a carbon source as the soil carbon is steadily increasing over the last two decades (Xie et al., 2007; Yu, Huang, & Zhang, 2012). Thus, we did not consider soil as a carbon source in this study. At present, fossil fuels consumption and cement production are the prime carbon emissions sources in Guangdong (Wang, Zhu, Liu, & Ma, 2010). Therefore, we took into account these two sources for calculating the carbon emissions of Guangdong. Specifically, the carbon emissions caused by energy consumption $C_{e,\mathrm{fossil}}$ was calculated using the following equation (IPCC, 2006):

$$C_{e,\mathrm{fossil}} = \sum_i E_i \times V_i \times c_i \quad (8)$$

where E_i is the physical consumption of fuel type i; V_i and c_i are the calorific value carbon emission factor of fuel type i. The calorific values and carbon emission factors of different fuel types (Dhakal, 2009) are shown in Table 1.

Cement production also can generate a large amount of carbon emissions through carbonate degradation. The carbon emissions from cement production $C_{e,\mathrm{cement}}$ was calculated as follows (IPCC, 2006):

$$C_{e,\mathrm{cement}} = q \times c \times e_{clc} \quad (9)$$

where q is the actual cement production (i.e., regional production plus cement importation minus cement exportation); c is the proportion of comprehensive clinker (set as 0.75 in accordance with (Wang et al., 2010)), and e_{clc} is the clinker carbon emission factor, set as 0.52 (t-C/t) (IPCC, 2006). The total regional carbon emissions is the sum of $C_{e,\mathrm{fossil}}$ and $C_{e,\mathrm{cement}}$.

The vegetation carbon sink was calculated based on the respective area and the carbon sink intensity of each vegetation type:

$$C_s = \sum C_{i,s} = \sum_j A_{i,j} \times v_j \quad (10)$$

where C_s is the total vegetation carbon sink, and $C_{i,s}$ is the carbon sink of pixel i; $A_{i,j}$ is the area of vegetation type j, and v_j is the carbon sink intensity vegetation type j. We determined the carbon sink intensity of each vegetation type based on previous related studies (Chen, Xu, Li, Fu, & Yan, 2012; Fang, Guo, Piao, & Chen, 2007): 0.7559 (t-C/ha yr^{-1}) for broad-leaved forest, 0.3662 (t-C/ha yr^{-1}) for coniferous forest, and 0.134 (t-C/ha yr^{-1}) for shrubland. The farmland ecosystem also can absorb some amount of atmospheric carbon, but its contribution to regional carbon sink is not significant because of the short harvest period of crops (Fang et al., 2007; Piao et al., 2009). Therefore, the value of carbon sink intensity for farmland was set to zero.

Study area and data

Guangdong Province is located in southern China, consisting of a total of 21 cities. These cities can be divided into four groups according to the cities' geographical locations (see Fig. 3), namely east flank cities, west flank cities, mountainous cities and the cities in the Pearl River Delta. Chaozhou, Shantou, Jieyang and Shanwei are east flank cities, while Zhanjiang, Maoming and Yangjiang are west flank cities. Cities in the north of the province, including Qingyuan, Shaoguan, Heyuan, Meizhou and Yunfu, are called mountainous cities because they are within the mountainous area. The rest of the cities, including Guangzhou, Foshan, Dongguan, Shenzhen, Zhongshan, Zhuhai, Huizhou, Jiangmen and Zhaoqing, compose the so-called Pearl River Delta region, which is the core economic region in Guangdong.

Guangdong is a typical humid sub-tropical area with annual mean precipitation of 1300–2500 mm. The raining season usually starts from April and ends around October. Cloudy days are frequent even in winter. Such weather condition makes it difficult to acquire cloud-free Landsat images. Fig. 3 shows the path/row numbers of all overpassed Landsat TM/ETM+ images for Guangdong in December, 2009. It is almost impossible to find all the overpassed Landsat images to be cloudless on similar acquisition dates. The percentage cloud cover of the overpassed images in the coast exceeds 40% on average, some even reaching 97%. The images covering the northern inland area are of better quality, with the percentage cloud cover of less than 20%. Thus, it is necessary to combine Landsat and MODIS images to obtain a better land-cover classification in Guangdong.

The MODIS and Landsat TM/ETM+ images were downloaded from the U.S. Geological Survey Earth Resources Observation and

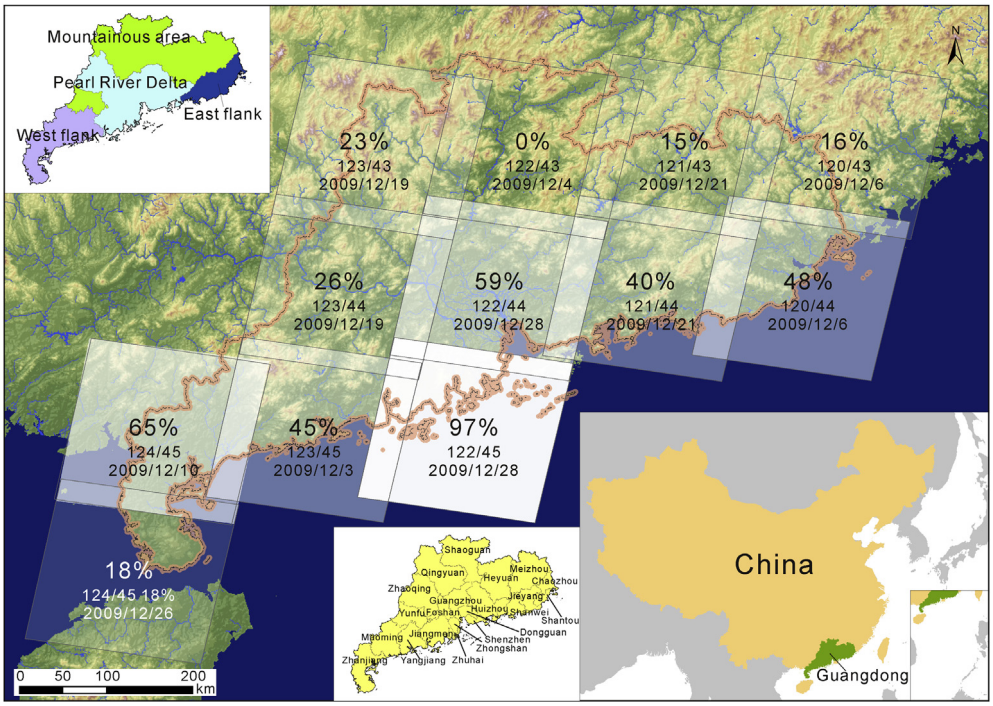

Fig. 3. The location of Guangdong Province, the path/row number and cloud cover of the overpassed Landsat TM/ETM+ images.

Science Center (http://glovis.usgs.gov/) and from the International Scientific Data Service Platform (http://datamirror.csdb.cn/). Two scenes of MODIS images were selected for the analysis in this study. They are the 8-day composited product (MOD09A1) of surface reflectance with a 500-m resolution. Their acquisition dates are December 26, 2000 and December 3, 2009. Because of the serious stripes, the fifth band of the selected MODIS images were abandoned during classification. Six scenes of 30-m Landsat TM/ETM+ images were used for sample collection and classification validation. The selection of the Landsat TM/ETM+ images followed these principles: the cloud cover should be as low as possible; the selected images should contain all the land-cover categories; the acquisition dates should be close to those of the selected MODIS images. The path/row number and acquisition dates of the selected Landsat TM/ETM+ images are: 120/44 (January 15, 2010), 121/044 (December 28, 2000), 121/43 (December 28, 2000), 122/044 (November 1, 2000 and November 2, 2009), and 122/43 (November 2, 2009). All of the downloaded MODIS and Landsat images had already been geo-referenced by the data providers. These data were all re-projected into the Universal Transverse Mercator (UTM) coordinate systems (zone 49N) using the WGS-84 (World Geodetic System 1984) ellipsoid.

The socio-economic data were collected from Guangdong Statistical Yearbook (Statistics Bureau of Guangdong Province, 2001, 2010), including provincial and city populations, provincial and city gross domestic products (GDP), and per capita GDP. The energy data were obtained from the Guangdong Energy Balance Sheet (Physical quantity) in China Energy Statistical Yearbook (2010).

Results and discussion

Implementation and validation of the MLA model

The parameter k (i.e., the number of neighbors) in Equation (5) is a key factor that influences the performance of the MLA model. Thus, we first repeatedly run the MLA model for several times to find an appropriate value of k. As demonstrated by Fig. 4, the classification error is inversely proportional to the value of k and tends to stabilize after k reaches 10. Therefore, k was set to 10 for subsequent applications. The results of the MLA model are shown in Figs. 5 and 6. The overall RMSE is 0.204 for year 2000 and 0.197 for 2009 (Table 2).

The results of the MLA model were compared with those of the frequently-used DT model – the model based on decision tree algorithm (C4.0). Because the DT model is a hard classification model, a pixel-hardening procedure should be carried out for the MLA model's results before comparison. The hardening of a pixel means to assign (only) one representative land-cover type to this pixel based on the given land-cover composition. This can be determined using the largest-area-rule, which means for any pixel, the land-cover type with largest areal proportion will be selected and assigned to this pixel as its label/class (Liu et al., 2010). This rule is problematic if a pixel contains two or more land-cover types with equal areal proportions. For instance, consider a pixel with three land-cover types, each of which has the same areal

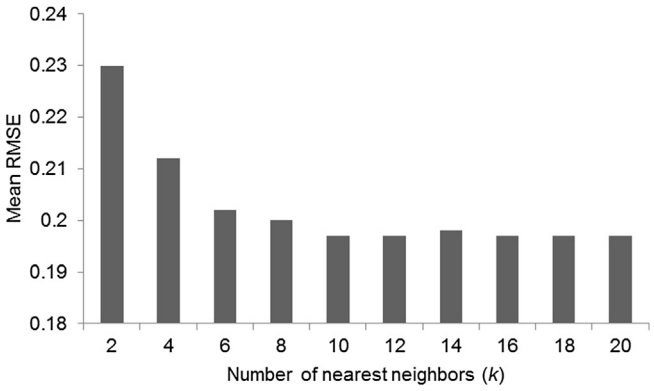

Fig. 4. The relationship between parameter k and RMSE.

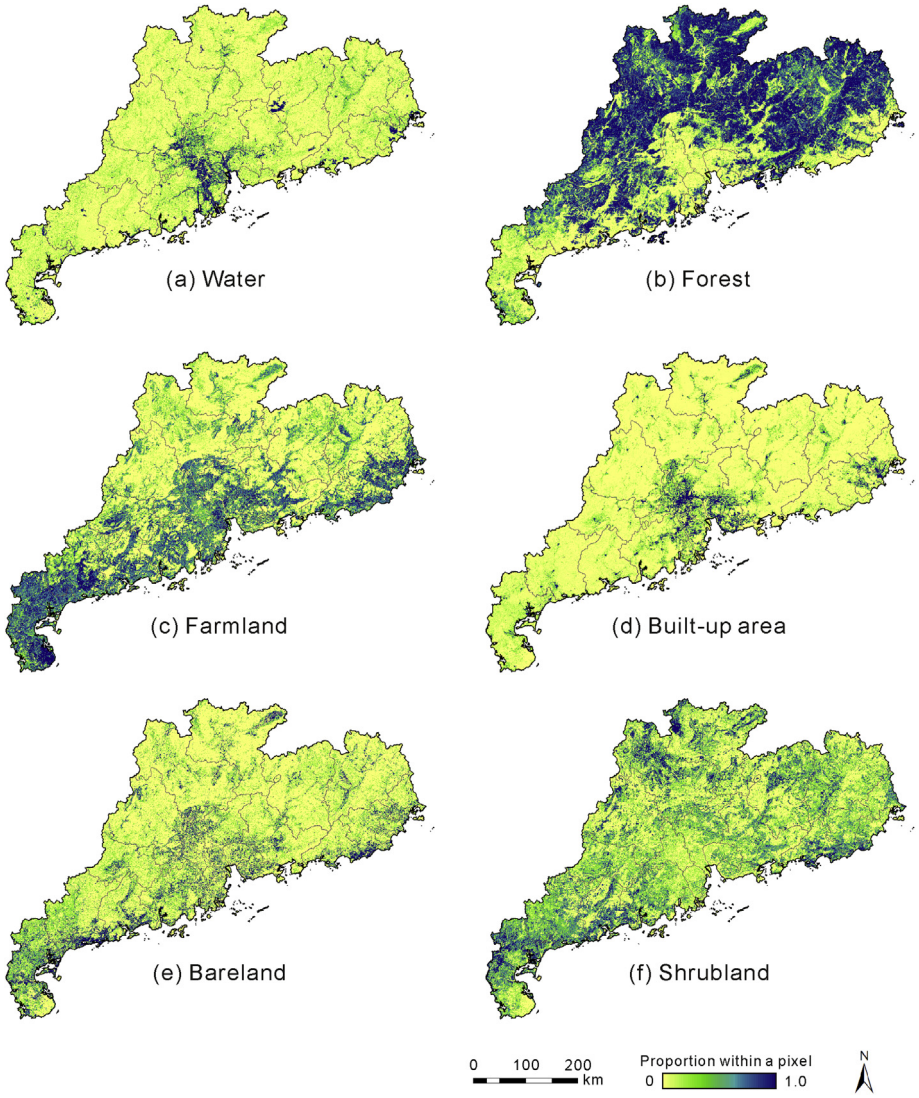

Fig. 5. Land-cover of Guangdong for year 2000 ('Broad-leaved forest' and 'Coniferous forest' were combined as 'Forest').

proportion of 1/3. In this case, none of these three types can become the "representative land-cover type" for this pixel. Thus, we refined the hardening rules as follows: for any pixel, if there is a land-cover type whose areal proportion exceeds 0.5, then the pixel should be labeled as that land-cover type; if there is no any land-cover type with a more-than-0.5 areal proportion, then this pixel is labeled as a "mixed" type. Fig. 7(a) and (b) shows the hardened results of the MLA model. The hardening procedure was also implemented for the collected samples. The hardened samples were then randomly divided into two groups: one was used to train the DT model, whereas the other was treated as test data.

Table 3 shows the classification accuracies of the MLA model and the DT model. The overall accuracies of the MLA model are quite low (less than 70%) if it is implemented in a hard classification manner. This is due to the contradiction between the core assumption of hard classification (single choice of class) and the existence of mixed-pixels on MODIS images. As a pixel on MODIS images usually consists of multiple land-cover types, it is difficult to assign an appropriate land-cover type for such a pixel.

Nevertheless, the overall accuracies of the MLA model are still 11%–14% higher than those of the DT model. This is because the MLA model has better ability than the DT model to utilize the information gained from Landsat images. The MLA model considers pixels as mixed rather than pure, and uses the *k*-nn algorithm to effectively handle the complicated relationship between the land-cover composition and the spectra. The rich information obtained from Landsat images can support the MLA model to accurately induce the land-cover composition of an unknown pixel on MODIS images. However, the DT model intrinsically regards any pixels, including the training samples, as pure ones. Therefore, the samples collected from Landsat images have to be hardened beforehand. This may discard a large amount of complementary information gained from Landsat images. Such information loss will inevitably affect the training of the DT model. Moreover, the DT model cannot capture the relationship between the land-cover composition and the spectra of those mixed-pixels. This is reflected by the DT model's extremely low classification accuracies of "mixed" type, as shown in Table 3.

Land-cover change and regional carbon budget

Table 4 shows the areal change of each land-cover type between 2000 and 2009. The built-up area in Guangdong grew from 6239.89 km^2 to 10,796.21 km^2 (increased by 73.01%). Forest land

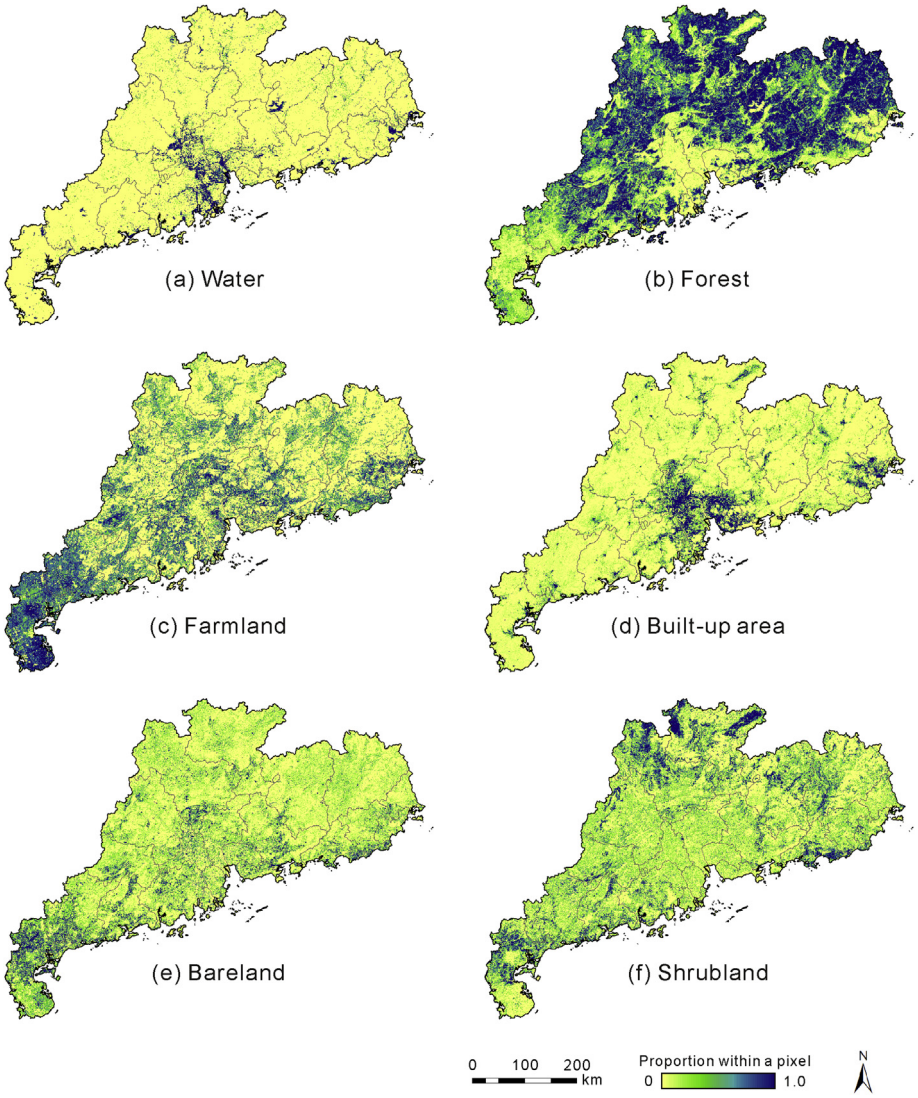

Fig. 6. Land-cover of Guangdong for year 2009 ('Broad-leaved forest' and 'Coniferous forest' were combined as 'Forest').

(including broad-leaved and conifer forests) had the biggest areal decrease among all land-cover types. However, the reduced area (2952.02 km^2) only accounted for 3.03% of the total forest land in 2000. Forest land remained as the largest land-cover type in 2009, with a land coverage of approximately 53%. Water body also reduced by 267.38 km^2 due to the coastal reclamation activities and the conversion of aquatic areas to built-up areas. The area of farmland changed slightly with a small reduction of 254.63 km^2, which accounted for 1.11% of the total farmland area in 2000.

Fig. 7(c) shows the land conversion between 2000 and 2009 based on the hardened results of the MLA model. New built-up areas were mainly concentrated in the center (the Pearl River Delta) and the east flank of Guangdong. In these two regions, farmland and water body were the immediate land sources for new built-up areas. However, a lot of forest land was converted into farmland in the west flank and parts of the Pearl River Delta. Therefore, the farmland loss due to urban expansion was partly covered by reclaiming forest land. Moreover, some forest land in the north of Guangdong was transformed into mixed land-cover type. This aggravated the areal loss of forest land in Guangdong.

From late 1980s to 2000s, the built-up area in Guangdong grew with an annual rate of around 8%–10% (Fan, Wang, & Wang, 2008; Seto & Kaufmann, 2003). In the period of 2000–2009, the growth rate decreased to 6.29% annually (Table 4), which was still a high rate. The per capita built-up area at provincial level increased from 72.14 km^2 to 112.02 km^2 (Table 5), indicating a trend of urban sprawl. Fig. 8(a) and (b) shows the per capita built-up area at city level in 2000 and 2009. It can be found that cities in the east and west flanks of Guangdong had lower per capita built-up area, whereas cities in the center and the north had higher per capita built-up area. Cities of Foshan, Jiangmen and Zhongshan, which had the highest per capita built-up area, continued their rapid growing trend in the past two decades (Fan et al., 2008; Li & Yeh, 2004). Those mountainous cities, such as Shaoguan and Heyuan, also had

Table 2
The root-mean-square errors (RMSE) of the land-cover classifications produced by the MLA model.

Year	W	BF	CF	FL	BA	BL	SL	Overall
2000	0.127	0.285	0.202	0.300	0.210	0.152	0.155	0.204
2009	0.153	0.263	0.146	0.304	0.199	0.131	0.185	0.197

Note: W = Water; BF = Broad-leaved forest; CF = Coniferous forest; FL = Farmland; BA = Built-up area; BL = Bareland; SL = Shrubland.

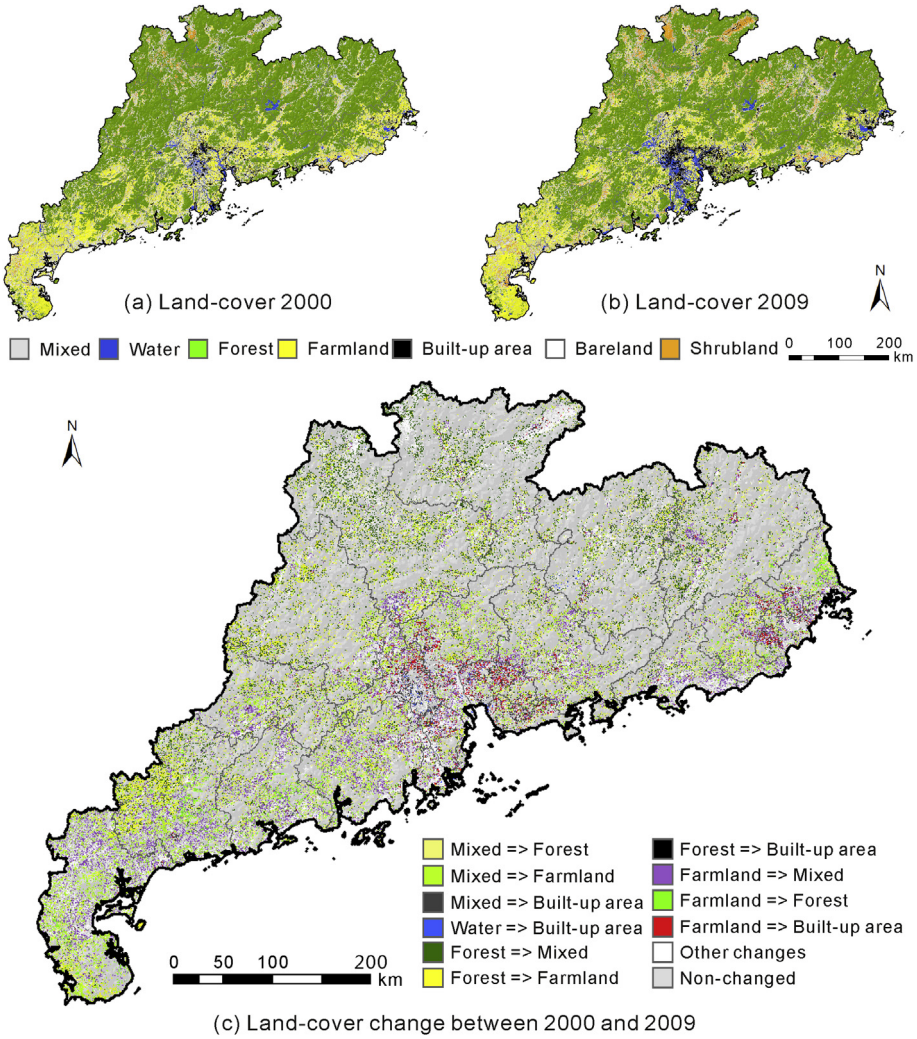

Fig. 7. (a)–(b) The hardened results of the MLA model's classification; (c) Land-cover change in Guangdong Province between 2000 and 2009.

very high per capita built-up area, mainly because these cities are in an early development stage and rely on heavy input of land resources to make economic returns.

The provincial land-use efficiency, represented by the GDP of per square kilometer of built-up area, improved from 172 million yuan/km^2 (≈$27.61 million/km^2) to 297 million yuan/km^2 (≈$47.67 million/km^2) with an annual increase of 6.26% (Table 5), nearly equal to the rate of urban expansion. The land-use efficiencies are the highest in the coastal cities (e.g. Shanwei, Shenzhen, Guangzhou, Zhuhai, and Yangjiang) and gradually decrease from these cities to the inland cities (e.g. Shaoguan, Qingyuan, and Heyuan) (Fig. 8(c) and (d)). Surprisingly, the land-use efficiencies in Foshan, Dongguan, and Huizhou are also below the provincial level. Although these cities are most developed in the Guangdong, they remain in a development stage of low land utilization level.

Table 3
Classification accuracies (%) of the MLA model and the DT model.

Year	W	BF	CF	FL	CA	BL	SL	M
MLA (Overall accuracy: 62.9% in year 2000; 65.1% in year 2009)								
2000	72.7	72.5	64.2	64.2	62.0	52.2	69.2	45.8
2009	79.6	73.3	68.4	60.7	79.1	52.9	53.8	52.8
DT (Overall accuracy: 48.3% in year 2000; 53.4% in year 2009)								
2000	78.3	65.0	31.9	45.9	65.4	46.2	39.1	14.6
2009	79.1	66.2	42.9	57.2	74.8	44.2	46.2	16.7

Note: W = Water; BF = Broad-leaved forest; CF = Coniferous forest; FL = Farmland; BA = Built-up area; BL = Bareland; SL = Shrubland; M = Mixed.

Impacts of land-cover change on regional carbon budget

Land-cover change has significant influences on regional carbon budget. The change of vegetation type and quantity affects the regional carbon sink. Urban expansion, economic development and population growth in all give rise to the increase of regional carbon emissions. In the following analysis, we further explore the impacts of land-cover change on regional carbon budget in Guangdong.

Fig. 9(a) and (b) show the spatial distributions of vegetation carbon sink in 2000 and 2009, respectively. The mountainous areas in the north of Guangdong have very high carbon sink because of the wide coverage of forest land, whereas the Pearl River Delta and

Table 4
Area (km^2) of each land-cover type in Guangdong.

Year	Water	Forest	Farmland	Built-up area	Bareland	Shrubland
2000	7919.33	97,289.18	36,917.44	6239.89	8117.93	21,124.60
2009	7651.95	94,337.16	36,662.81	10,796.21	7271.7	20,888.54
Change	−267.38	−2952.02	−254.63	4556.32	−846.23	−236.06

Table 5
Statistics of built-up area in Guangdong in 2000 and 2009.

Year	Coverage of the province (%)	Per capital built-up area (km^2)	Land-use efficiency (million yuan/km^2)
2000	3.51	72.14	172 (≈$27.61)
2009	6.08	112.02	297 (≈$47.67)

Note: The GDP in 2009 was converted based on the price in 2000.

the plains in the east and west flanks have much lower carbon sink as their major land-cover types are farmland and shrubland.

As shown in Table 6, forest land contributed most of the carbon sink in Guangdong (95.86% in 2000 and 95.89% in 2009). Owing to the reduction of forest land, the vegetation carbon sink dropped from 7.01 million t-C to 6.82 million t-C between 2000 and 2009. Fig. 9(c) reveals that there was a notable decrease of carbon sink in the mountainous area and the west flank due to the conversion of forest land into farmland and other land-cover types (Fig. 7(c)). By contrast, carbon sink increased in some small hilly areas near the eastern border of the province because of the restoration of forest land.

We also aggregated the change of carbon sink into city level to show a clearer pattern (Fig. 9(d)). The highest increase of vegetation carbon sink is found in the west flank cities, such as Zhanjiang, Yanjiang and Jiangmen. There is also a slight increase of vegetation carbon sink in the east flank cities (e.g. Chaozhou and Jieyang). The most serious reduction of carbon sink is witnessed in the mountainous cities (Zhaoqing, Qingyuan, Shaoguan, and Heyuan), even though they still have abundant forest land.

Compared with the slight decrease of vegetation carbon sink, there was an astonishing increase of carbon emissions between 2000 and 2009 (Table 7). The carbon emissions from energy consumption in 2009 were 129.29 million t-C, more than double the emissions in 2000. This is due to the undergoing fast industrialization and economic development from 2000 to 2009. According to the provincial statistics yearbook (Statistics Bureau of Guangdong Province, 2010), 66.9% of the total provincial energy consumption was spent in the secondary industry in 2009. The fossil-fuels-dominant energy structure is another cause of the increased carbon emissions. Although the usage of total raw coal and crude oil decreased from 87.2% to 72.3%, fossil fuels remained as the main source of energy in 2009 (Statistics Bureau of Guangdong Province, 2010). The provincial energy demand is expected to accelerate as the industrialization will continue in the future (Kuby, He, Trapido-Lurie, & Moore, 2011). But the associated growth of carbon emissions can somewhat be offset if the energy structure is improved, such as increasing the use of hydropower, sunlight or nuclear power.

The carbon emissions generated by cement production also grew very fast (increased by approximately 71%) between 2000 and 2009 because of the rapid urbanization and related land construction. The expansion of urban areas stimulates the demand of cement for constructions of residential, industrial/commercial buildings and other infrastructures. Although the share of carbon emissions from cement production dropped to 23.2% in 2009, such proportion still exceeded the national average of 7.2–12.0% (Wang et al., 2010). Regarding that at present cement production in China is still relatively inefficient, the problem of carbon emissions may be exacerbated because of the growing demand of cement driven by future urban expansion (Güneralp & Seto, 2012).

The energy efficiency was improved from 2000 to 2009, as indicated by the declined carbon emissions per unit GDP (see Table 8). However, such improvement was not large enough to effectively stabilize the provincial carbon emissions (Table 7). The per capita carbon emissions also increased almost 90% in this period (from 0.92 t-C to 1.74 t-C, see Table 8). This is related to the growing personal wealth over the last decade. Previous research demonstrated that the increase of personal wealth encourages people to change their life styles into the ones that are more energy intensive, such as the ownership of automobiles (Dieleman, Dijst, & Burghouwt, 2002). Actually, the number of private cars can grow even faster than the GDP in some cities of Guangdong (Y. Chen et al.,

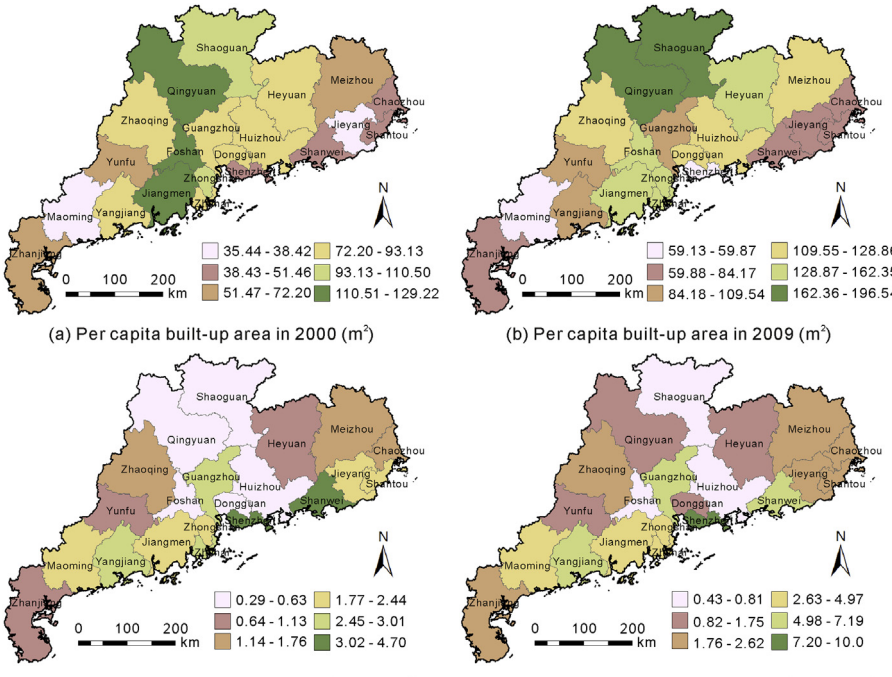

Fig. 8. Per capital built-up area and land-use efficiency for each city in Guangdong Province.

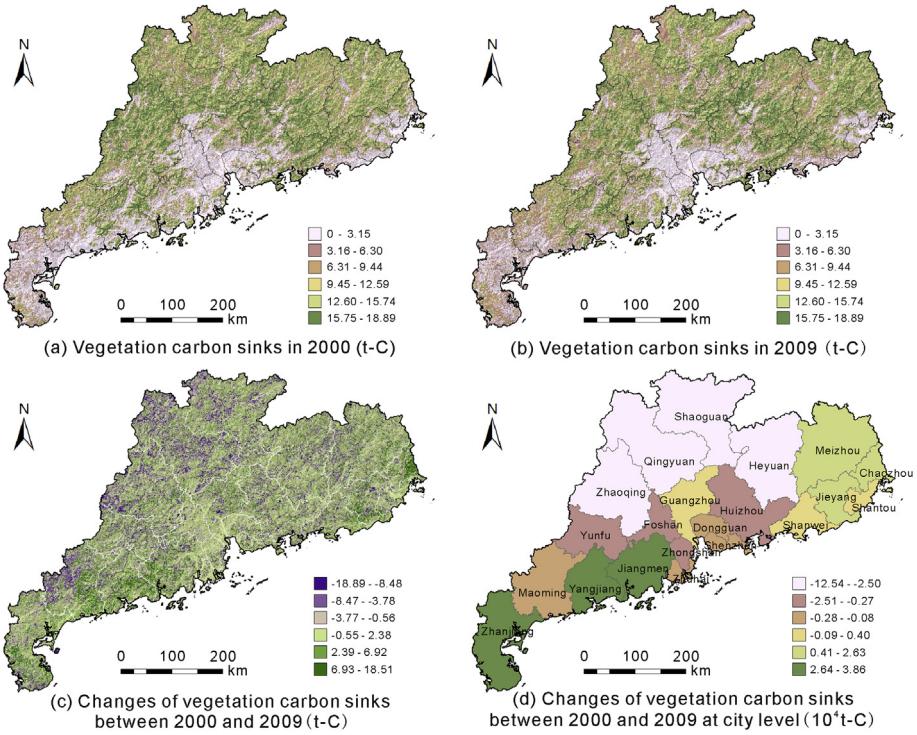

Fig. 9. The spatial distribution and the change of vegetation carbon sink in Guangdong from 2000 to 2009.

2011). The recent provincial per capita carbon emissions are still lower than those in developed countries such as USA (around 4.8 t-C) or Japan (around 2.5 t-C). But it would become devastating if the per capita emissions reach the similar levels of these countries because of the large population in Guangdong. The carbon emissions per square built-up area also increased by 22.8% from 2000 to 2009 (Table 8). In fact, as indicated by Güneralp and Seto (2012), efforts have been made to reduce the demand of materials and energy for individual buildings in the cities of Guangdong, but the gains in efficiency were outstripped by the fast expansion of built-up areas and hence failed to slow down the regional carbon emissions.

In year 2000, the vegetation carbon sink could offset 8.8% of total carbon emissions of Guangdong. This level was just a little lower than that of the East Asia region at the same period, in which about 10.9% of the annual carbon emissions could be absorbed by vegetation (Ito, 2008). However, the vegetation carbon sink of Guangdong could only offset 4.1% of its total carbon emissions in 2009, far below the national level (approximately 7.0–7.7%) (Fang et al., 2007; Wang et al., 2010). Ma and Wang (2011) believe that Guangdong still has large space for afforestation and thus has high potential for increasing the regional vegetation carbon sink. According to their forecasts, the cumulative amount of forest carbon sink from 2005 to 2050 is 389.23 million t-C, i.e., 8.65 million t-C yr^{-1} on average. Such level of annual forest carbon sink only accounted 5.1% of the total carbon emissions in 2009. Therefore, it is not enough to improve the regional carbon budget merely by afforestation.

More measures should be taken with respect to the control of land development as urban expansion have strong impacts on the regional carbon budget. In China, land development is a crucial factor to sustain domestic economic growth (Deng, Huang, Rozelle, & Uchida, 2010). Local governments in some Chinese cities have also realized the importance of regulating urban expansion for retaining environmental quality and the sustainability of future development. For instance, the cities of Dongguan and Shenzhen, which locate in the Pearl River Delta, start to establish their ecological protection areas to restrict urban sprawl (Li, Lao, Liu, & Chen, 2011). The immediate benefit from these protection efforts is the conservation of important ecological services, such as absorbing the atmospheric carbon. Meanwhile, land development can also be controlled so that the associated growth of resources demand (e.g. energy) might be stabilized. In addition, promoting the compactness of urban forms can effectively reduce urban energy consumption. This has been confirmed by several empirical studies in American cities (National Academy of Sciences of United States, 2009). Two recent researches in Asian cities also suggest that fragmented and sprawled urban forms consume more energy than compact urban forms (Chen et al., 2011; Makido, Dhakal, & Yamagata, 2012).

Conclusions

Our study has demonstrated the necessity of combining various sources of satellite images to derive land-cover data for Guangdong

Table 6
Vegetation carbon sink of Guangdong in 2000 and 2009 (million t-C).

Year	Forest carbon sink	Shrubland carbon sink	Total carbon sink
2000	6.72	0.29	7.01
2009	6.54	0.28	6.82
Change	−0.18	−0.01	−0.19

Table 7
Carbon emissions of Guangdong in 2000 and 2009 (million t-C).

Year	Carbon emission from energy consumption	Carbon emission from cement production	Total carbon emission
2000	56.65	22.90	79.55
2009	129.29	39.11	168.40
Change	72.64	16.21	88.85

Table 8
Per capita carbon emissions, carbon emissions per unit GDP, and carbon emissions per square built-up area of Guangdong in 2000 and 2009.

Year	Per capita carbon emissions (t-C)	Carbon emissions per unit GDP (t-C/10^4 yuan)	Carbon emissions per square built-up area (10^4 t-C/km^2)
2000	0.92	0.74	1.27
2009	1.74	0.53	1.56

Note: The GDP in 2009 was converted based on the price in 2000.

Province, a large humid sub-tropical region in China. Cloudy and rainy weather in Guangdong raises the difficulties of obtaining cloudless Landsat images. It is almost impossible to acquire all the cloudless overpassed Landsat images on similar dates because of the relatively long revisit time of Landsat. MODIS images have much shorter revisit frequency and hence become another image source. We integrated MODIS images with available cloudless Landsat images for land-cover classification based on the MLA model. As a soft classification model, the MLA model is more suitable for the classification of MODIS images because of its ability to deal with mixed-pixels problem.

The analysis of land-cover change reveals that forest land in Guangdong decreased by 3.03% from 2000 to 2009, while built-up area rapidly expanded by 73.01% in the same period. Farmland was the major land source for urban development during this period. But the overall reduction of farmland was marginal because a fraction of forest land was converted into farmland. At the provincial level, the land-use efficiency increased by 6.26% annually, almost equal to the urban growth rate (6.29%). Due to the declined vegetation area, the vegetation carbon sink decreased by 0.19 million t-C, which accounted for 2.6% of the carbon sink in 2000. However, the total carbon emissions increased by more than 100% from 2000 to 2009 because of the rapid urban development. The vegetation carbon sink can only offset 4.1% of total carbon emissions in 2009, far below the national level (around 7.0–7.7%).

In this study, we neglected the influences of soil carbon stocks and soil respiration when estimating the regional carbon budget. Recent studies found that the soil carbon stocks in Guangdong increase by 1.17 million t-C annually (Xie et al., 2007), which is quite small compared with the amount of carbon emissions (168.40 million t-C in 2009). Thus, the estimated carbon budget may not change a lot if soil carbon stocks and soil respiration are taken into account in this study. Nevertheless, these sources will be examined in our future study to provide a comprehensive pattern of carbon budget in Guangdong. We will also explore the spatial connections between urban expansion and regional carbon budget in future study. Although empirical studies consistently reveal a significant relationship between urban forms and urban carbon emissions, the mechanism behind this relationship is rather complex and needs further examination (National Academy of Sciences of United States, 2009). Additionally, local governments of many Chinese cities are aware of the importance of establishing policies to adjust the structure of urban economy for stabilizing the energy consumption (Dhakal, 2009). Thus, models will also be developed to evaluate the potential impacts of such polices on urban development and associated energy/carbon consequences.

Acknowledgments

We thank the three anonymous reviewers for their useful comments and suggestions. This research was supported by the National Basic Research Program of China (973 Program) (grant no. 2011CB707103), and the National Natural Science Foundation of China (grant no. 41371376 and 41171308).

References

Canadell, J. G., Le Quéré, C., Raupach, M. R., Field, C. B., Buitenhuis, E. T., Ciais, P., et al. (2007). Contributions to accelerating atmospheric CO_2 growth from economic activity, carbon intensity, and efficiency of natural sinks. *Proceedings of the National Academy of Sciences, 104*(47), 18866.

Chen, Y., Li, X., Zheng, Y., Guan, Y., & Liu, X. (2011). Estimating the relationship between urban forms and energy consumption: a case study in the Pearl River Delta, 2005–2008. *Landscape and Urban Planning, 102*(1), 33–42.

Chen, Q. Q., Xu, W. Q., Li, S. G., Fu, S. L., & Yan, J. H. (2012). Aboveground biomass and corresponding carbon sequestration ability of four major forest types in south China. *Chinese Science Bulletin, 57*(13), 1119–1125.

Deng, X., Huang, J., Rozelle, S., & Uchida, E. (2010). Economic growth and the expansion of urban land in China. *Urban Studies, 47*(4), 813–843.

Dhakal, S. (2009). Urban energy use and carbon emissions from cities in China and policy implications. *Energy Policy, 37*(11), 4208–4219.

Dieleman, F., Dijst, M., & Burghouwt, G. (2002). Urban form and travel behaviour: micro-level household attributes and residential context. *Urban Studies, 39*(3), 507–527.

Evrendilek, F., Berberoglu, S., Karakaya, N., Cilek, A., Aslan, G., & Gungor, K. (2011). Historical spatiotemporal analysis of land-use/land-cover changes and carbon budget in a temperate peatland (Turkey) using remotely sensed data. *Applied Geography, 31*(3), 1166–1172.

Fang, J. Y., Guo, Z. D., Piao, S. L., & Chen, A. P. (2007). Terrestrial vegetation carbon sinks in China, 1981–2000. *Science In China Series D: Earth Sciences, 50*(9), 1341–1350.

Fan, F., Wang, Y., & Wang, Z. (2008). Temporal and spatial change detecting (1998–2003) and predicting of land use and land cover in core corridor of Pearl river delta (China) by using TM and ETM+ images. *Environmental Monitoring and Assessment, 137*(1), 127–147.

Foody, G. M. (1997). Fully fuzzy supervised classification of land cover from remotely sensed imagery with an artificial neural network. *Neural Computing & Applications, 5*(4), 238–247.

Foody, G. M. (2000). Estimation of sub-pixel land cover composition in the presence of untrained classes. *Computers & Geosciences, 26*(4), 469–478.

Friedl, M., McIver, D., Hodges, J., Zhang, X., Muchoney, D., Strahler, A., et al. (2002). Global land cover mapping from MODIS: algorithms and early results. *Remote Sensing of Environment, 83*(1–2), 287–302.

Gao, F., Masek, J., Schwaller, M., & Hall, F. (2006). On the blending of the Landsat and MODIS surface reflectance: predicting daily Landsat surface reflectance. *IEEE Transactions on Geoscience and Remote Sensing, 44*(8), 2207–2218.

Güneralp, B., & Seto, K. C. (2012). Can gains in efficiency offset the resource demands and CO_2 emissions from constructing and operating the built environment? *Applied Geography, 32*(1), 40–50.

Hilker, T., Wulder, M. A., Coops, N. C., Seitz, N., White, J. C., Gao, F., et al. (2009). Generation of dense time series synthetic Landsat data through data blending with MODIS using a spatial and temporal adaptive reflectance fusion model. *Remote Sensing of Environment, 113*(9), 1988–1999.

Hutyra, L. R., Yoon, B., Hepinstall-Cymerman, J., & Alberti, M. (2011). Carbon consequences of land cover change and expansion of urban lands: a case study in the Seattle metropolitan region. *Landscape and Urban Planning, 103*(1), 83–93.

Intergovernmental Panel on Climate Change. (2006). In *IPCC guidelines for national greenhouse gas inventories* (Vol. 3). Kanagawa, Japan.

Ito, A. (2008). The regional carbon budget of East Asia simulated with a terrestrial ecosystem model and validated using AsiaFlux data. *Agricultural and Forest Meteorology, 148*(5), 738–747.

Kuby, M., He, C., Trapido-Lurie, B., & Moore, N. (2011). The changing structure of energy supply, demand, and CO_2 emissions in China. *Annals of the Association of American Geographers, 101*(4), 795–805.

Latifovic, R., Zhu, Z. L., Cihlar, J., Giri, C., & Olthof, I. (2004). Land cover mapping of North and Central America—global land cover 2000. *Remote Sensing of Environment, 89*(1), 116–127.

Leckie, D. G. (1990). Advances in remote sensing technologies for forest surveys and management. *Canadian Journal of Forest Research, 20*(4), 464–483.

Li, X., Lao, C., Liu, X., & Chen, Y. (2011). Coupling urban cellular automata with ant colony optimization for zoning protected natural areas under a changing landscape. *International Journal of Geographical Information Science, 25*(4), 575–593.

Lin, W., Zhang, L., Du, D., Yang, L., Lin, H., Zhang, Y., et al. (2009). Quantification of land use/land cover changes in Pearl river delta and its impact on regional climate in summer using numerical modeling. *Regional Environmental Change, 9*(2), 75–82.

Liu, K., Li, X., Shi, X., & Wang, S. G. (2008). Monitoring mangrove forest changes using remote sensing and GIS data with decision-tree learning. *Wetlands, 28*(2), 336–346.

Liu, X., Li, X., & Zhang, X. (2010). Determining class proportions within a pixel using a new mixed-label analysis method. *IEEE Transactions on Geoscience and Remote Sensing, 48*(4), 1882–1891.

Liu, S., Loveland, T. R., & Kurtz, R. M. (2004). Contemporary carbon dynamics in terrestrial ecosystems in the southeastern plains of the United States. *Environmental Management, 33*, 442–456.

Li, X., & Yeh, A. G. O. (2004). Analyzing spatial restructuring of land use patterns in a fast growing region using remote sensing and GIS. *Landscape and Urban Planning, 69*(4), 335–354.

Makido, Y., Dhakal, S., & Yamagata, Y. (2012). Relationship between urban form and CO_2 emissions: evidence from fifty Japanese cities. *Urban Climate, 2*, 55–67.

Ma, X. Z., & Wang, Z. (2011). Estimation of provincial forest carbon sink capacities in Chinese mainland. *Chinese Science Bulletin, 56*(9), 883–889.

National Academy of Sciences of United States. (2009). *Driving and the built environment: The effects of compact development on motorized travel, energy use, and CO_2 emissions*. Washington, DC: Transportation Research Board of the National Academies.

National Bureau of Statistics. (2010). *China energy statistical yearbook 2010*. Beijing, China: China Statistics Press.

Piao, S., Fang, J., Ciais, P., Peylin, P., Huang, Y., Sitch, S., et al. (2009). The carbon balance of terrestrial ecosystems in China. *Nature, 458*(7241), 1009–1013.

Potter, C. (2010). The carbon budget of California. *Environmental Science & Policy, 13*(5), 373–383.

Redo, D. J., & Millington, A. C. (2011). A hybrid approach to mapping land-use modification and land-cover transition from MODIS time-series data: a case study from the Bolivian seasonal tropics. *Remote Sensing of Environment, 115*(2), 353–372.

Seto, K., & Kaufmann, R. (2003). Modeling the drivers of urban land use change in the Pearl river delta, China: integrating remote sensing with socioeconomic data. *Land Economics, 79*(1), 106.

Seto, K., Woodcock, C., Song, C., Huang, X., Lu, J., & Kaufmann, R. (2002). Monitoring land-use change in the Pearl river delta using Landsat TM. *International Journal of Remote Sensing, 23*(10), 1985–2004.

Shen, J., Wong, K., & Feng, Z. (2002). State-sponsored and spontaneous urbanization in the Pearl river delta of south China, 1980–1998. *Urban Geography, 23*(7), 674–694.

Statistics Bureau of Guangdong Province. (2001). *Guangdong statistical yearbook 2001*. Beijing, China: China Statistical Press.

Statistics Bureau of Guangdong Province. (2010). *Guangdong statistical yearbook 2010*. Beijing, China: China Statistical Press.

Sulla-Menashe, D., Friedl, M. A., Krankina, O. N., Baccini, A., Woodcock, C. E., Sibley, A., et al. (2011). Hierarchical mapping of Northern Eurasian land cover using MODIS data. *Remote Sensing of Environment, 115*(2), 392–403.

Sun, J., Wang, X., Chen, A., Ma, Y., Cui, M., & Piao, S. (2011). NDVI indicated characteristics of vegetation cover change in China's metropolises over the last three decades. *Environmental Monitoring and Assessment, 179*(1), 1–14.

Turner, B. L., Lambin, E. F., & Reenberg, A. (2007). The emergence of land change science for global environmental change and sustainability. *Proceedings of the National Academy of Sciences, 104*(52), 20666–20671.

Wang, W., Kuang, Y., & Huang, N. (2011). Study on the decomposition of factors affecting energy-related carbon emissions in Guangdong province, China. *Energies, 4*(12), 2249–2272.

Wang, Z., Zhu, Y., Liu, C., & Ma, X. (2010). Integrated projection of carbon emission for China under the optimal economic growth path. *Acta Geographica Sinica, 65*(12), 1559–1568.

Wessels, K., De Fries, R., Dempewolf, J., Anderson, L., Hansen, A., Powell, S., et al. (2004). Mapping regional land cover with MODIS data for biological conservation: examples from the Greater Yellowstone Ecosystem, USA and Pará State, Brazil. *Remote Sensing Of Environment, 92*(1), 67–83.

Xie, Z., Zhu, J., Liu, G., Cadisch, G., Hasegawa, T., Chen, C., et al. (2007). Soil organic carbon stocks in China and changes from 1980s to 2000s. *Global Change Biology, 13*(9), 1989–2007.

Yu, Y., Huang, Y., & Zhang, W. (2012). Modeling soil organic carbon change in croplands of China, 1980–2009. *Global and Planetary Change, 82*, 115–128.